Available online at BCREC website: https://bcrec.id

Bulletin of Chemical Reaction Engineering & Catalysis, 15 (3) 2020, 641-652

Research Article

Effect of FSP-inserted Cu on Physicochemical Properties of Cu/Al_2O_3 Catalyst

Charuwan Poosri[1], Choowong Chaisuk[1,*], Wantana Klysubun[2]

[1]Department of Chemical Engineering, Faculty of Engineering and Industrial Technology, Silpakorn University, Nakhon Pathom 73000, Thailand.
[2]Synchrotron Light Research Institute, 111 University Ave., Muang, Nakhon Ratchasima 30000, Thailand.

Received: 18th June 2020; Revised: 7th August 2020; Accepted: 10th August 2020; Available online: 26th August 2020; Published regularly: December 2020

Abstract

The copper inserted on Cu/Al_2O_3 catalysts with various Cu loading (10-40 wt%) were synthesized via flame spray pyrolysis (FSP). These catalysts were characterized using X-ray diffraction (XRD), N_2 physisorption, temperature programmed reduction (TPR) and X-ray absorption near edge spectroscopy (XANES). The XRD results confirmed the formation of copper aluminate spinel ($CuAl_2O_4$) on the FSP-inserted Cu catalyst. The CuO crystallite size of the Cu/Al_2O_3 catalysts was increased with increasing Cu loading during the flame spray pyrolysis step. The incorporation of copper and aluminum precursors during the flame spray pyrolysis step can inhibit the growth of Al_2O_3 particles resulting in higher BET surface area and smaller particle size than pure Al_2O_3 support. The data from TPR and XANES results can predict the ratio of CuO and $CuAl_2O_4$ in the FSP-made support. Less than 20 wt% loading of the FSP-inserted Cu showed high concentration of $CuAl_2O_4$ phase in the FSP-made material. The composition of CuO and $CuAl_2O_4$ phase can be controlled by varying Cu loading in flame spray pyrolysis step. This is a promising alternative way to synthesize the desired catalyst. An example was the catalytic testing of the selective hydrogenolysis of glycerol. The presence of both CuO and $CuAl_2O_4$ phases in the Cu/Al_2O_3 catalyst enhanced the catalytic activity and promoted the selectivity to acetol product.

Keywords: Flame spray pyrolysis (FSP); Cu/Al_2O_3; $CuAl_2O_4$ spinel; $CuO/CuAl_2O_4$ ratio

How to Cite: Poosri, C., Chaisuk, C., Klysubun, W. (2020). Effect of FSP-inserted Cu on Physicochemical Properties of Cu/Al_2O_3 Catalyst. *Bulletin of Chemical Reaction Engineering & Catalysis*, 15(3), 641-652 (doi:10.9767/bcrec.15.3.8193.641-652)

Permalink/DOI: https://doi.org/10.9767/bcrec.15.3.8193.641-652

1. Introduction

Nowadays, the copper-based materials are widely used in several applications. These are electrical conductors, ceramic-reinforced composites and catalysts. In the field of catalyst, the copper-based catalysts play important roles in many commercial catalytic processes including hydrogenation, hydrodeoxygenation, water gas shift (WGS), methane decomposition, methanol reforming reaction, NO reduction and fine chemical processing. They show high activity and selectivity since copper prefers cleavage of the C−OH bond to obtain desired products but declines cleavage of the C−C bond [1−3]. The copper particles can be dispersed on the support, especially metal oxides such as Al_2O_3, SiO_2, TiO_2, and ZnO. In particular, an alumina supported copper catalyst (Cu/Al_2O_3) is a widespread catalyst due to its acid strength,

* Corresponding Author.
E-mail: CHAISUK_C@su.ac.th (C. Chaisuk);
Telp: +66-81-4203022, Fax: +66-34-252459

high thermal stability and high surface for active metal loading. An example is the use of this catalyst for glycerol hydrogenation that shows two steps to produce propylene glycol. This reaction required both acidic and metallic sites for converting glycerol to acetol and producing propylene glycol from acetol, respectively [4,5]. In general, the catalytic property mostly depends on condition of process and nature of catalyst. A morphology of the catalyst particle, an interaction with the support and an atomic structure on the catalyst surface affect significantly the catalytic performance. Many forms of Cu-containing species, *e.g.* metals, oxides, alloys and spinels, can be valid as the active sites. Many observations have suggested that the different form of Cu species on the catalyst surface related to the catalytic activity. It was reported that the participation of Cu^0, Cu^+, and Cu^{2+} surface species enhanced hydrogenation of dienes and methanol synthesis [6–8], while only Cu^0 surface was active for CO hydrogenation [9]. On the other hand, the copper aluminate species ($CuAl_2O_4$) had promotional effect in glycerol hydrogenolysis, methanol stream reforming, benzyl alcohol oxidation and photocatalytic degradation of organic pollutants [10–14].

The catalysts containing desired forms of Cu species are obtained by a wide variety of preparation techniques such as impregnation, sol-gel method, and co-precipitation. Recently, the copper supported on alumina was prepared by a novel chemical reduction method. It was found that the Cu metal was the main species of Cu/Al_2O_3 catalyst and the Cu_2O was slightly produced by oxidation of Cu metal on the surface [15]. Shim *et al.* [16] synthesized CeO_2 promoted $Cu/\gamma\text{-}Al_2O_3$ catalyst by co-impregnation and sequential impregnation method. They reported that the catalyst preparation techniques affected the transformation of bulk Cu species to cluster Cu species, and the catalytic performance for high temperature water gas shift reaction. Morales-Leal and coworkers [17] suggested that the $CuAl_2O_4$ species was apparent on the catalyst surface when the Cu/Al_2O_3 catalyst was calcined at temperature beyond 500 °C. The presence of $CuAl_2O_4$ showed high catalytic activity for methanol-ethanol oxidation. Wolosiak-Hnat *et al.* [18] mentioned that the $CuAl_2O_4$ phase gave good catalytic activity in glycerol hydrogenolysis to 1,2-propanediol. From the above information, the synthesis of suitable Cu forms on the catalyst surface benefits the development of catalyst field. One of popular synthesis methods is the flame spray pyrolysis (FSP). The simultaneous metal oxides and spinels can be prepared by this method in a single step. The phase composition of both was adjusted by various parameters such as precursor concentration, precursor feed rate and precursor composition [19,20]. Granados *et al.* [21] found that the addition of cobalt and aluminum in liquid precursor resulted in the formation of cobalt aluminate spinel ($CoAl_2O_4$) and cobalt oxides (CoO) phases. Kim et al. [22] noted that the Ce-Al-O system with 5-10 mol% CeO_x concentration appeared both cerium oxide (CeO_2) and cerium magnetoplumbite spinel structure ($CeAl_{11}O_{18}$).

The metal aluminate spinel has been synthesized by several techniques, *e.g.* co-precipitation, so-gel method, solid state fusion method and microwave irradiation method [23–26]. However, the aluminate spinel was generally obtained at high calcination temperature about 1000 °C for several days in order that the spinel phase was completely formed. This was difficult to scaling up of synthesis and economic perspective. The flame spray pyrolysis (FSP) was an established commercial process to prepare metal-oxide spinel in a single step [27,28]. The FSP products with low contaminated compounds were made at high temperature (up to 3000 K) [29]. Moreover, the characteristic of these products can be controlled by fuel composition, precursor feed rate, precursor concentration and type of precursor *etc.* [30,31]. In this work, the Cu/Al_2O_3 catalysts were synthesized by two sequential methods. The FSP-made material was prepared using mixed copper and aluminum precursors and then the copper was again impregnated on this material. The Cu content in the FSP-made material was varied to obtain the different phase composition. The Cu/Al_2O_3 catalysts were characterized by N_2 physisorption, inductively coupled plasma (ICP), X-ray diffraction (XRD), X-ray absorption near edge structure (XANES) and temperature programmed reduction (TPR).

2. Materials and Methods

2.1 Material Synthesis

A series of FSP-made material were prepared by varying the Cu content in a range of 0-40 wt%. The flame spray pyrolysis reactor is shown in Figure 1. The starting precursors were copper (II) acetylacetonate (Sigma-Aldrich, 97 wt%) and aluminum-tri-sec-

butoxide (Sigma-Aldrich, 98 wt%). These precursors were diluted with xylene to 0.5 M solution. This liquid solution was fed with 5 ml/min into the center capillary of nozzle using a syringe pump and dispersed into spray by 5 L/min of oxygen. The pressure drop at the nozzle was held constant at 1.5 bar. A supporting premixed methane and oxygen with 1.5 and 3.2 L/min of gas flow rates, respectively, ignited and stabilized the flame. A sinter metal ring surrounding the flame was supplied by an additional 5 L/min of sheath oxygen flow. The powder product was collected on a glass microfiber filter (Diameter 150 mm, Whatman) with the aid of a vacuum pump. This product was addressed as the *x*Cu-Al_2O_3 support. The *x* symbol meant the weight percentage of Cu based on the support material. All of the *x*Cu-Al_2O_3 supports were impregnated by the Cu. The impregnated Cu loading was 10 wt% based on the whole material. A copper (II) nitrate trihydrate (Sigma-Aldrich, 98 wt%) was dissolved in deionized water and mixed with the *x*Cu-Al_2O_3 support. The slurry was stirred at 70 °C for 6 h to obtain the paste. This paste was dried overnight at 110 °C and subsequently calcined at 400 °C for 3 h in airflow. The obtained material was addressed as the Cu/*x*Cu-Al_2O_3 catalyst.

2.2 Material Characterization

The pore characteristics and BET surface area of the catalyst were evaluated by the N_2 physisorption using BET DORP mini II. The catalyst was pretreated in a helium gas flow of 50 ml/min at 220 °C for 3 h to remove moisture in the solid particle. Analysis was measured at −196 °C with N_2 gas. The specific surface areas were determined by the BET multipoint method with relative pressure of 0.001−0.20. The average particle size was calculated using $D_{BET} = 6000/(\rho \times S_{BET})$, where D_{BET} was the particle diameter (nm), ρ was the powder density (g/cm^3), and S_{BET} was specific surface area (m^2/g). The XRD patterns were performed on X-Ray Diffractometer Bruker AXS Model D8 Discovere using Cu-Kα radiation (λ = 1.5406 Å). The diffractograms were recorded from 10 to 80° 2θ using a scanning rate of 2°/min, scan speed of 0.3 sec/step with operating voltage and current of 40 kV and 40 mA, respectively. The crystallite size was estimated from line broadening according to the Scherrer equation as follows: crystallite size = K·λ/B·cosθ, where K = 0.9 (crystallite-shape factor), λ = 1.5418 Å for Cu Kα (wavelength of X-ray) and B was X-ray diffraction broadening. The bulk reduction behavior of each catalyst was studied by H_2 temperature programmed reduction using a Micromeritics Pulse Chemisorb 29100 instrument. A 0.1 g of catalyst samples in a quartz tubular reactor was initially heated under 30 ml/min of nitrogen flow at a rate of 10 °C/min to 150 °C and then held at this temperature for 1 h. After cooled down to room temperature by nitrogen, the reducing gas (10% H_2 in N_2) was switched on at 30 ml/min, and the temperature was raised at a rate of 10 °C/min until it reached 800 °C. The XANES spectra Cu K-edge was performed on the beamline BL8 at Synchrotron Light Research

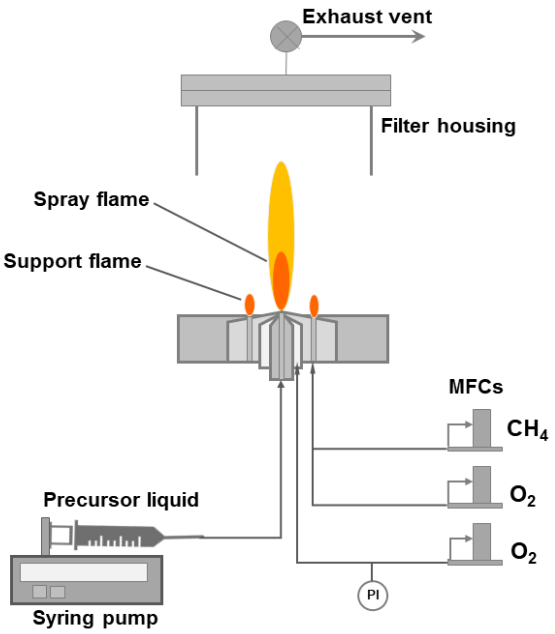

Figure 1. Scheme of flame spray pyrolysis.

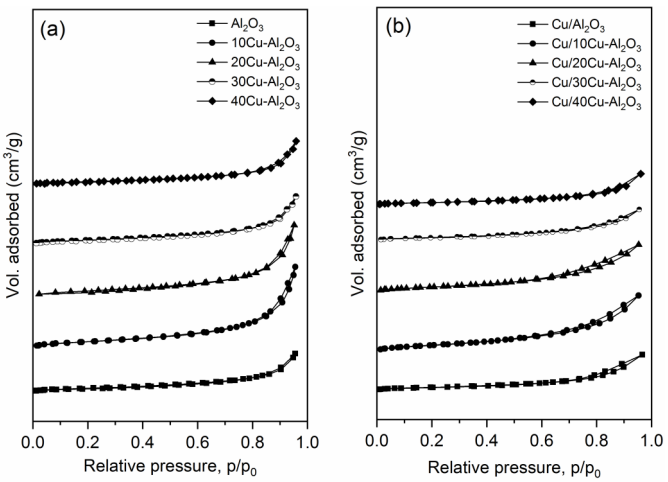

Figure 2. The N_2 adsorption/desorption isotherms of the (a) *x*Cu-Al_2O_3 prepared by FSP and, (b) Cu/*x*Cu-Al_2O_3, (x= 10, 20, 30, 40 wt%).

Institute (SLRI), Thailand [32]. The XANES data were measured in transmission mode and then analyzed by the Athena - program [33].

3. Results and Discussions

3.1 N_2 Adsorption/desorption Isotherms

The N_2 adsorption/desorption isotherms and pore size distribution of the xCu-Al_2O_3 supports and the Cu/xCu-Al_2O_3 catalysts are shown in Figures 2 and 3, respectively. The FSP-made Al_2O_3 support displayed the typical type II N_2 adsorption according to IUPAC classification indicating most of macroporous structure. The addition of 30 and 40 wt% Cu during the flame spray pyrolysis step hardly affected the characteristics of the pore structure. On the other hand, at 10 and 20 wt% Cu, the hysteresis loop indicating mesoporous structure was apparent. These were H3-type

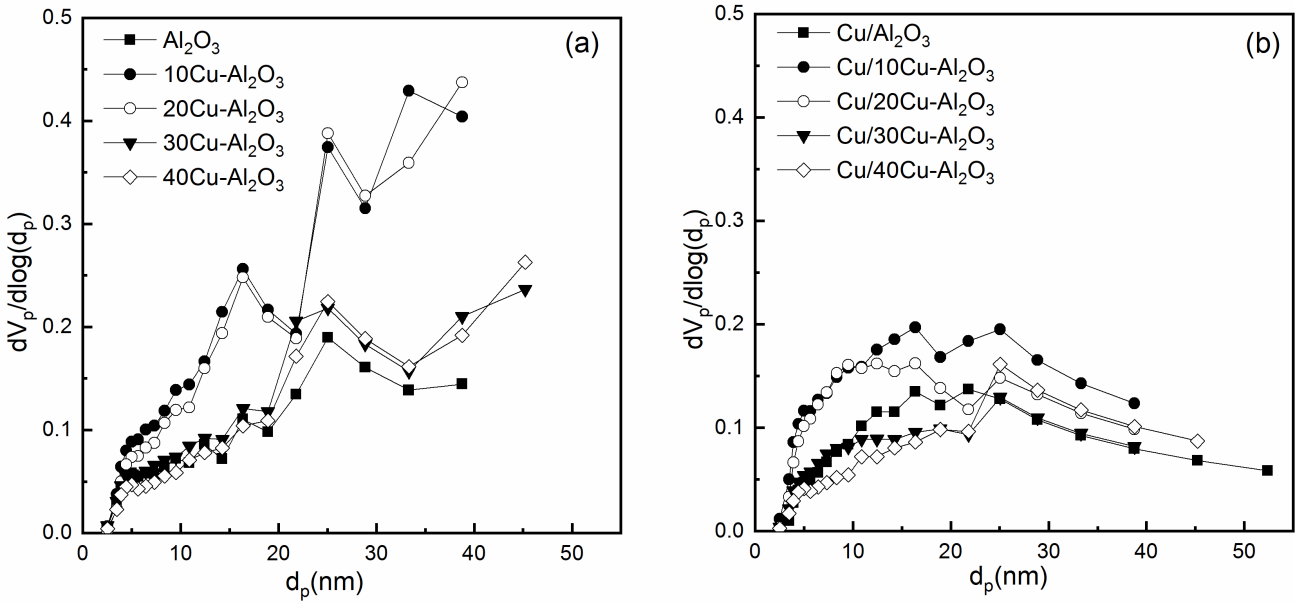

Figure 3. The pore size distribution of (a) xCu-Al_2O_3 prepared by FSP and, (b) Cu/xCu-Al_2O_3, (x= 10, 20, 30, 40 wt%).

Table 1. The physical properties of Cu/Al_2O_3.

Samples	Cu content (wt%)[a]	Surface area (m^2/g)[b]	Total pore volume	Particle size (nm)[c]	CuO crystallite size (nm)[d]
Al_2O_3	-	37	0.11	44	-
10Cu-Al_2O_3	11.0	94	0.24	17	n.d
20Cu-Al_2O_3	19.5	66	0.28	24	13.6
30Cu-Al_2O_3	32.6	42	0.14	39	15.9
40Cu-Al_2O_3	42.6	33	0.13	49	19.0
Cu/Al_2O_3	-	30	0.11	54	20.3
Cu/10Cu-Al_2O_3	-	69	0.17	24	22.0
Cu/20Cu-Al_2O_3	-	57	0.14	29	24.6
Cu/30Cu-Al_2O_3	-	33	0.09	49	26.3
Cu/40Cu-Al_2O_3	-	27	0.09	59	26.6

[a] Determined by ICP technique; [b] Determined by BET method; [c] Calculated by the following equation: Particle size (nm) = 6000/(S_{BET}.ρ), where S_{BET} is surface area of sample (m^2/g), and ρ is density of sample (g/cm^3); [d] Calculated from XRD results

hysteresis loop that were characteristic of aggregates of plate-like particles or slit-shaped pores. Figure 3(a) also confirms that the pores with size less than 40 nm was abundant on the 10Cu-Al_2O_3 and 20Cu-Al_2O_3 supports. The pore distribution of *x*Cu-Al_2O_3 supports exhibited the multimodal pore size.

After the impregnation of 10 wt% Cu on the *x*Cu-Al_2O_3 supports, the amount of multilayer adsorbed N_2 was clearly decreased but the pore characteristics were similar. This was due to plugging the pores by impregnated Cu particles [34], which was consistent with loss of the pores in size range less than 40 nm as shown in Figure 3(b). The BET surface area and the pore volume of all the materials are shown in Table 1. The average particle size was also calculated from the BET data. The specific surface area was significantly increased when 10-20 wt% Cu was introduced during the flame spray pyrolysis step. It was indicated that the Cu dopant disturbed the formation of Al_2O_3 by inhibiting the growth of Al_2O_3 particles. This was in agreement with the catalyst synthesis by doping some metals during the flame spray pyrolysis step [35−37]. However, a large amount of Cu showed low BET surface area because the Cu particles aggregated themselves to form larger particles.

3.2 X-Ray Diffraction

The *x*Cu-Al_2O_3 samples were characterized by X-ray diffraction technique as shown in Figure 4. The diffraction peaks at 2θ = 32.0°, 39.0°, 45.8° and 66.5° corresponding to the characteristic of γ-Al_2O_3 were observed for all catalysts. The other works previously reported that the alumina with γ-Al_2O_3 phase can be easily synthesized by the flame spray pyrolysis technique [37−40]. Insertion of 10 wt% of copper with Al_2O_3 during the flame spray pyrolysis step displayed the characteristic peaks of copper aluminate phase ($CuAl_2O_4$) at 2θ = 32.0°, 37.4°, 45.5°, 56.3°, 60.0° and 65.9°. When the 20 wt% Cu was introduced during the flame spray pyrolysis step, the tiny peaks of CuO was apparent together with the main peaks of $CuAl_2O_4$. The CuO peaks were located at 32.5°, 35.6°, 38.8°, 48.8°, 53.5°, 58.3°, 61.6°, 66.2°, 68.1°, 72.4°, and 75.2° according to the reflections from (−110), (002), (111), (202), (020), (202), (−113), (−311), (113), (311) and (−222) planes of CuO monoclinic structure (JCPDS #PDF45-09370), respectively [41]. A high Cu content (30 and 40 wt%) showed the very sharp peaks of both $CuAl_2O_4$ and CuO phases. The stoichiometric content of Cu to form $CuAl_2O_4$ was 38 wt% and therefore CuO was simply produced by excess Cu. The crystallite size of CuO particles became larger with increasing Cu loading. This crystallite size calculated from XRD data according to the Scherrer's equation is listed in Table 1. Figure 5 shows the XRD pattern of the Cu/*x*Cu-Al_2O_3 samples. The Al_2O_3-supported Cu catalyst exhibited the diffraction peaks of only CuO and γ-Al_2O_3. The $CuAl_2O_4$ phase was not apparent in this case. It was implied that the impregnated Cu did not react with Al_2O_3 to form the $CuAl_2O_4$ phase. The sharp peaks assigned as the CuO phase were certainly observed on all the Cu/*x*Cu-Al_2O_3 catalysts. This indicated that the amount of CuO particles was increased by the impregnation of Cu on the FSP-made catalysts.

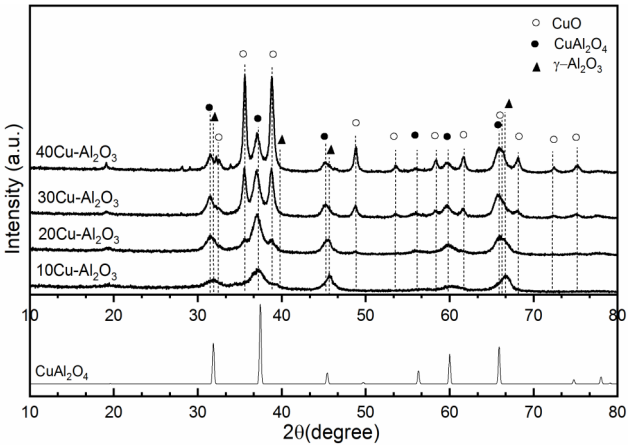

Figure 4. The XRD patterns of *x*Cu-Al_2O_3 samples prepared by FSP, (*x* = 10, 20, 30, 40 wt%).

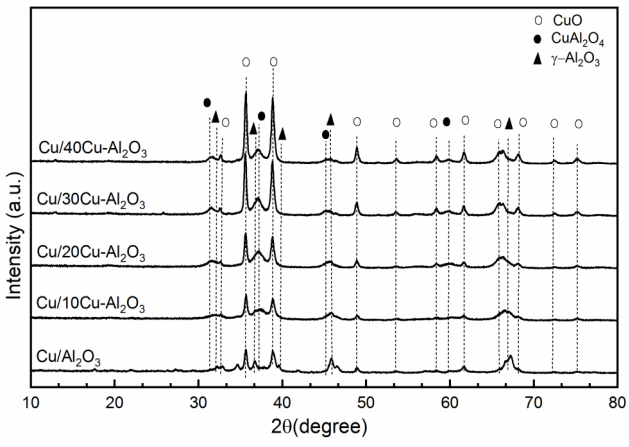

Figure 5. The XRD pattern of Cu/*x*Cu-Al_2O_3 samples, (*x*= 10, 20, 30, 40 wt%).

3.3 H_2 Temperature Programmed Reduction

The reduction behavior of the xCu-Al_2O_3 supports is shown in Figure 6. Two reduction regions were proposed by deconvolution. The first region addressed as the α zone was at low temperature below 300 °C. This attributed to the overlap of two reduction steps of CuO to Cu_2O and then Cu metal. These CuO species were well dispersed and weakly interacted with the alumina matrix [42,43]. This was consistent with a general reduction by H_2 of the bulk CuO in a temperature range of 200−450 °C [44]. When increasing copper loading, the hydrogen consumption in α region was increased. This related to a large amount of copper oxides on the catalyst surface. Moreover, the peaks in α region were shifted to higher temperature with increasing copper loading. It was implied that the particle sizes of copper oxides became larger consistent with the CuO crystallite size calculated from XRD results as shown in Table 1. The copper oxide particles with large sizes was more difficultly reduced than those with small sizes [34,45].

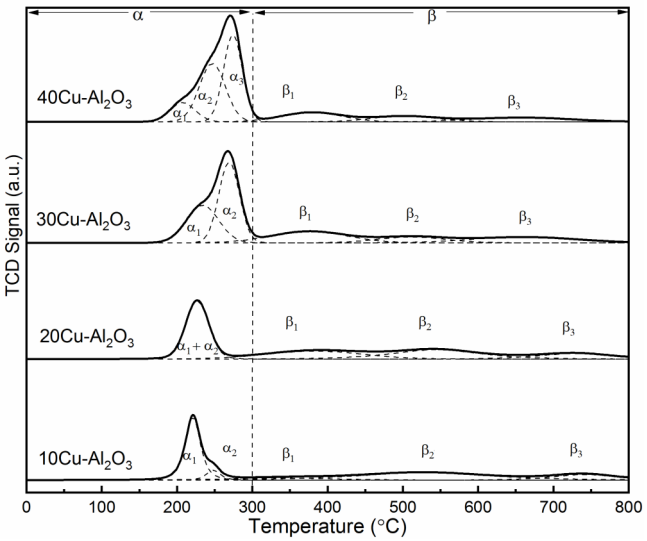

Figure 6. TPR patterns of xCu-Al_2O_3 samples prepared by FSP, (x = 10, 20, 30, 40 wt%).

The second reduction region assigned as the β zone was occurred at high temperature above 300 °C. The peaks were rather broad indicating the reduction of $CuAl_2O_4$ spinel structure. This structure is confirmed by the XRD results in Figure 4. In general, the bulk $CuAl_2O_4$ species was initially reduced at 400 °C until completely at 900 °C because of the strong interaction between metal and support [46]. The degree of reduction (DOR) calculated from the area under TPR profiles is presented in Table 2. This value was based on the theoretical loading of Cu in each catalyst. It was found that at 10 and 20 wt% Cu loading of the support, the H_2 consumption ratio of α and β regions was almost in the same level. This implied the same behavior of formation of segregated CuO and $CuAl_2O_4$ during the flame spray pyrolysis step for low Cu loading. It was also remarked that the 10Cu-Al_2O_3 showed higher DOR than the 20Cu-Al_2O_3. An increase of Cu loading from 20 to 40 wt% resulted an increase of the H_2 consumption ratio of α and ß region. It was indicated that the segregated

Table 2. The TPR result.

Samples	DOR of α peak from total (%)	DOR of β peak from total (%)	Ratio of α/β peak	Total DOR (%)	DOR (%) After pretreatment in H_2 at 300 ºC, 3 h	DOR (%) After pretreatment in H_2 at 400 ºC, 3 h
10Cu-Al_2O_3	49	51	1.0	76	-	-
20Cu-Al_2O_3	60	40	1.5	59	-	-
30Cu-Al_2O_3	78	22	3.6	70	-	-
40Cu-Al_2O_3	85	15	5.7	56	-	-
Cu/Al_2O_3	100	0	0	74	-	-
Cu/10Cu-Al_2O_3	68	32	2.1	71	-	-
Cu/20Cu-Al_2O_3	67	33	2.0	64	-	-
Cu/30Cu-Al_2O_3	81	19	4.2	63	-	-
Cu/40Cu-Al_2O_3	85	15	5.7	54	8	6

CuO was easily formed and its agglomeration was inevitable. Much more excess of Cu loading exhibited strong interaction of large CuO particles and alumina.

Figure 7 presents the TPR profiles of the Cu/*x*Cu-Al_2O_3 catalysts. Without loading Cu in the flame spray pyrolysis step, the Cu/Al_2O_3 catalyst showed two reduction peaks at 240 and 290 °C. This attributed to two reduction steps of dispersed CuO species to Cu_2O and then metallic copper. The TPR pattern was changed when the Cu was impregnated on the *x*Cu-Al_2O_3 supports. The reduction of CuO in the α region was completed at higher temperature. Several α peaks in a wide temperature range indicated the CuO with different particle sizes dispersed on the catalyst surface.

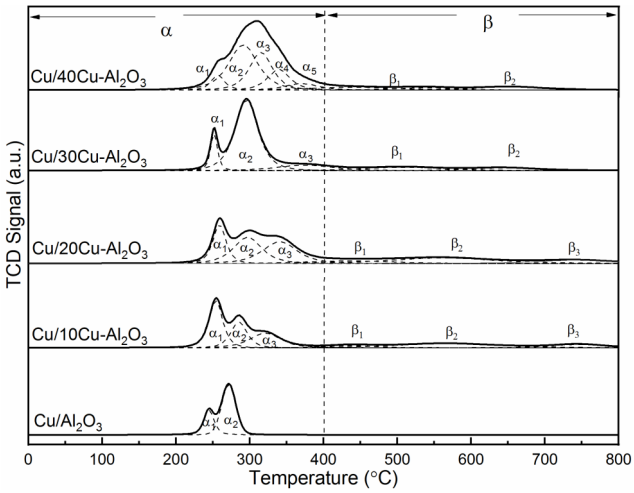

Figure 7. TPR patterns of Cu/*x*Cu-Al_2O_3 sample, (*x*= 0, 10, 20, 30, 40 wt%).

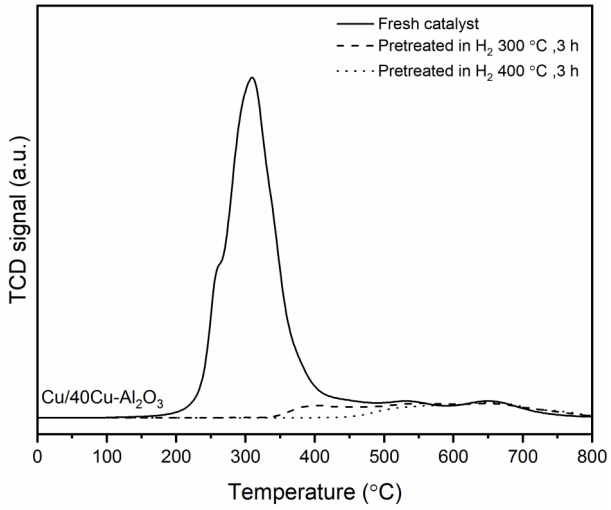

Figure 8. The comparison of TPR profiles of Cu/40Cu-Al_2O_3 fresh catalyst and pretreated catalyst at 300 ºC and 400 ºC under H_2 ambient flow for 3 h.

However, it was proposed that the reduction behavior of $CuAl_2O_4$ species in the β region was still similar. An addition of impregnated Cu in each support showed high DOR in α region. Before the catalytic testing, the Cu-based catalyst was generally reduced in the temperature range of 300−400 °C under H_2 flow to obtain metal active sites. Figure 8 demonstrates the comparative TPR profiles of the Cu/40Cu-Al_2O_3 catalyst before and after reduction. The fresh catalyst was reduced at 300 and 400 °C under H_2 ambient flow for 3 h. The peak in α region observed for the fresh catalyst was disappeared after reduction at both temperatures. It was implied that the CuO species can be reduced to metallic Cu particles on the catalyst surface. On the other hand, the presence of broad peaks in β region for three catalysts indicated a difficult reduction of $CuAl_2O_4$ species and therefore before the reaction, the catalyst surface contained both dispersed Cu metals and $CuAl_2O_4$ species. Based on the $CuAl_2O_4$ species in the reduced catalyst at 300 °C, there was about 75% remaining $CuAl_2O_4$ in that at 400 °C as shown in Table 2.

3.4 X-ray Absorption Near Edge Structure

Figure 9(a) shows the X-ray absorption near edge structure (XANES) spectra of the FSP-inserted Cu synthesized by flame spray pyrolysis. All samples exhibited similar XANES spectra. The XANES spectra displayed a weak pre-edge band around 8977 eV owing to the 1s→3d electronic transition corresponding to a tetrahedral Cu^{2+} species. The post-edge exhibited around 8987 to 8999 eV attributed to the 1s→4p electronic transition [47−49]. The

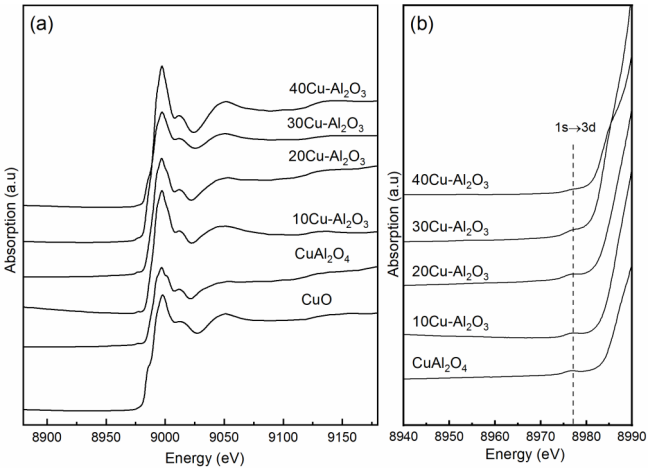

Figure 9. XANES spectra Cu K-edge of *x*Cu-Al_2O_3 prepared by FSP, (*x*= 10, 20, 30, 40 wt%).

intensity of the pre-edge peak of the xCu-Al_2O_3 samples decreased with increasing copper loading as shown Figure 9(b) because of a decrease of Cu^{2+} ions in tetrahedral site. The $CuAl_2O_4$ was a spinel structure with Cu^{2+} ions in tetrahedral site and Al^{3+} ions in octahedral site. In addition, the Cu K-edge of high copper loading was closer with the CuO standard, where a XANES spectra around 8987 eV was observed. Meanwhile, the addition of 10 wt% Cu on the FSP-made supports showed nearly the CuO standard, revealing the Cu^{2+} oxidation state as shown in Figure 10.

The XANES linear combination fit was used for investigating the composition of Cu species in the xCu-Al_2O_3 samples as presented in Table 3. The formation of $CuAl_2O_4$ was preferred at 20 wt% loading of the FSP-inserted Cu. The composition ratio of copper oxide and copper aluminate was again shown in Figure 11. This ratio was dramatically increased when more than 20 wt% Cu was loaded by the flame spray pyrolysis. From the TPR results, the catalytic reduction in the α and ß regions was speculated to the presence of copper oxide and copper aluminate, respectively. The DOR in each region was converted to be the weight of each copper species and then the mass ratio of copper oxide and copper aluminate was calculated. The relationship of this ratio and the Cu loading had a same tendency with the XANES results. It was indicated that the postulation from the TPR data was reliable.

A low mass ratio of $CuO/CuAl_2O_4$ composition obtained by the 10 and 20 wt% Cu loading related to a large content of copper aluminate. The mass ratio of $CuO/CuAl_2O_4$ was increased with increasing copper loading during flame spray pyrolysis. These results speculated that the interaction between CuO species and Al_2O_3 support became weaken with increasing the Cu loading. This could be explained by the growth of copper oxide particle via sintering process during flame spray pyrolysis process. A high copper loading could lower surface contact between copper oxide and alumina and therefore collision between copper oxides were easily occurred at high temperature. As shown in Figure 12, when the particles are rapidly cooled, a low

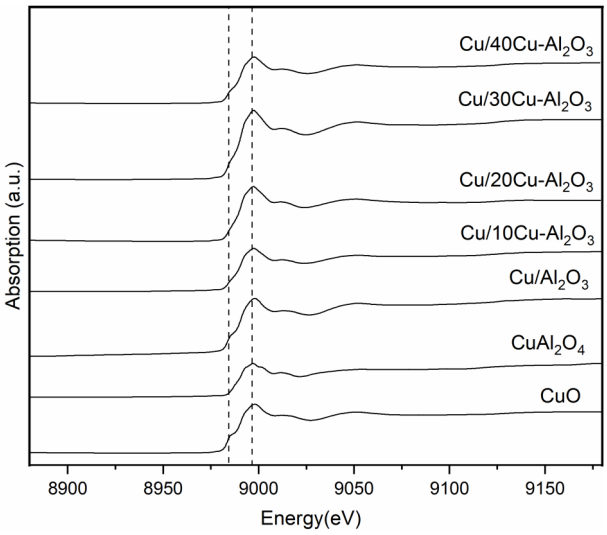

Figure 10. XANES spectra Cu K-edge of Cu/xCu-Al_2O_3 samples, (x = 0, 10, 20, 30, 40 wt%).

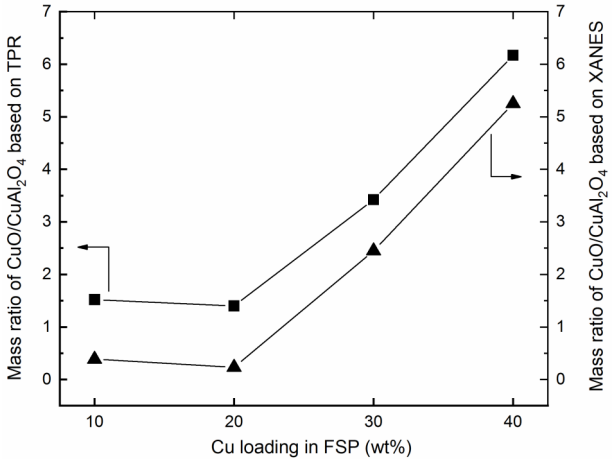

Figure 11. The mass ratio of copper oxide with alumina from XANES data and TPR data of xCu-Al_2O_3 prepared by FSP, (x = 0, 10, 20, 30, 40 wt%).

Table 3. The XANES results of xCu-Al_2O_3 samples prepared by flame spray pyrolysis.

Samples	Components		$CuO/CuAl_2O_4$ ratio
	CuO	$CuAl_2O_4$	
10Cu-Al_2O_3	0.28	0.72	0.39
20Cu-Al_2O_3	0.19	0.81	0.23
30Cu-Al_2O_3	0.71	0.29	2.45
40Cu-Al_2O_3	0.84	0.16	5.25

*XANES analysis by linear combination fit analysis.

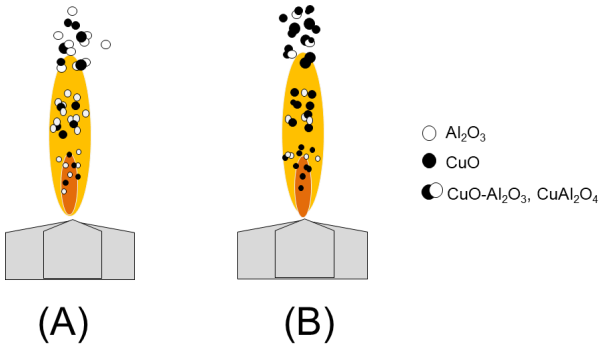

Figure 12. Schematics of FSP process for insertion of (A) low copper content with alumina and (B) high copper content with alumina.

metal loading has more effective to form metal-aluminate by flame spray pyrolysis method than a high metal loading. Form these results, a desired $CuO/CuAl_2O_4$ mass ratio can be obtained by adjusting Cu loading during flame spray pyrolysis step.

3.5 The Catalytic Testing by Selective Hydrogenolysis of Glycerol

The catalytic property of FSP-made Cu catalysts was evaluated by glycerol hydrogenolysis reaction in a batch reactor. The benchmark was 30 wt% Cu impregnated on the FSP-made Al_2O_3 support addressed as the $30Cu/Al_2O_3$. The BET surface area of this catalyst was 19 m^2/g. For comparison, total Cu loading of the selected catalysts was fixed as 30 wt%. These catalysts were $30Cu\text{-}Al_2O_3$ and $Cu/20Cu\text{-}Al_2O_3$. The catalytic activity and selectivity for selective hydrogenolysis of glycerol over three catalysts are shown in Figure 13. Comparing to the $30Cu/Al_2O_3$, both $30Cu\text{-}Al_2O_3$ and $Cu/20Cu\text{-}Al_2O_3$ catalysts displayed higher glycerol conversion and acetal selectivity. It was also remarked that both catalysts with FSP-inserted Cu showed the same trend of product distribution. It was reported that the catalytic pathway in glycerol hydrogenolysis was occurred through glycerol dehydration to acetol on acidic sites, acetol hydrogenation to 1,2-propnaediol on metallic copper, and then decomposition of 1,2-propanediol to propanal [50–52]. From this result, the presence of $CuAl_2O_4$ spinel on the catalyst surface can promote the acetol production and inhibit the 1,2-propanediol decomposition. Therefore, the catalyst modification by the FSP-inserted Cu was promising alternative way to enhance the desired reaction.

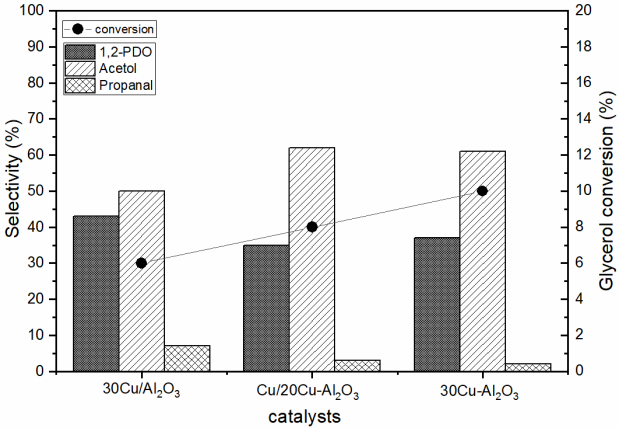

Figure 13. Catalytic testing for selective hydrogenolysis of glycerol. (Reference condition: 20 mL of 20 wt% aqueous glycerol solution, 0.2 g of reduced catalyst, 220 °C, 20 bar of H_2, 3 h).

4. Conclusion

The insertion of Cu in the Cu based catalysts by flame spray pyrolysis was studied. Incorporation of Cu and Al precursors during the flame spray pyrolysis can produce both CuO and $CuAl_2O_4$ phases while the addition of impregnated Cu on the FSP-made Al_2O_3 showed only CuO phase. The formation of $CuAl_2O_4$ was occurred by the flame spray pyrolysis. The FSP-inserted Cu inhibited the alumina growth as a consequence of high specific surface area. The specific surface area was decreased while the crystallite size of Cu was increased with increasing the FSP-inserted Cu loading. A large amount of FSP-inserted Cu showed a weaken interaction between copper oxide with alumina support. The XANES result indicated that a large amount of $CuAl_2O_4$ was formed at 10-20 wt% loading of the FSP-inserted Cu. For the application of catalyst field, the presence of both CuO and $CuAl_2O_4$ particles on the catalyst surface showed higher activity for glycerol hydrogenolysis and promoted the formation of acetol product. The composition of CuO and $CuAl_2O_4$ phases on the catalyst surface can be adjusted by varying the FSP-inserted Cu loading and therefore the flame spray pyrolysis was promising technique to synthesize the Cu based catalyst for the desired reaction.

Acknowledgment

The authors would like to thank Department of Chemical Engineering, Faculty of Engineering and Industrial Technology, Silpakorn University and Graduate School for financial support. In addition, the

experimental support of Synchrotron Light Research Institute (SLRI) beamline BL8 team, Thailand for the XANES analysis was acknowledged.

References

[1] Huang, Z., Cui, F., Kang, H., Chen, J., Xia, C. (2009). Characterization and catalytic properties of the CuO/SiO_2 catalysts prepared by precipitation-gel method in the hydrogenolysis of glycerol to 1,2-propanediol: Effect of residual sodium. *Applied Catalysis A: General*, 366, 288-298. DOI: 10.1016/j.apcata.2009.07.017.

[2] Sánchez, T., Salagre, P., Cesteros, Y., Bueno-López, A. (2012). Use of delaminated hectorites as supports of copper catalysts for the hydrogenolysis of glycerol to 1,2-propanediol. *Chemical Engineering Journal*, 179, 302-311. DOI: 10.1016/j.cej.2011.11.011.

[3] Mitta, H., Seelam, P.K., Ojala, S., Keiski, R. L., Balla, P. (2018). Tuning Y-zeolite based catalyst with copper for enhanced activity and selectivity in vapor phase hydrogenolysis of glycerol to 1,2-propanediol. *Applied Catalysis A: General*, 550, 308-319. DOI: 10.1016/j.apcata.2017.10.019.

[4] Kusunoki, Y., Miyazawa, T., Kunimori, K., Tomishige, K. (2005). Highly active metal–acid bifunctional catalyst system for hydrogenolysis of glycerol under mild reaction conditions. *Catalysis Communications*, 6, 645-649. DOI: 10.1016/j.catcom.2005.06.006.

[5] Mai, C.T.Q., Ng, F.T.T. (2016). Effect of metals on the hydrogenolysis of glycerol to higher value sustainable and green chemicals using a supported HSiW catalyst. *Organic Process Research & Development*, 20, 1774-1780. DOI: 10.1021/acs.oprd.6b00245.

[6] Xiao, Z., Wang, X., Xiu, J., Wang, Y., Williams, C.T., Liang, C. (2014). Synergetic effect between Cu^0 and Cu^+ in the Cu-Cr catalysts for hydrogenolysis of glycerol. *Catalysis Today*, 234, 200-207. DOI: 10.1016/j.cattod.2014.02.025.

[7] Delannoy, L., Thrimurthulu, G., Reddy, P.S., Méthivier, C., Nelayah, J., Reddy, B.M., Louis, C. (2014). Selective hydrogenation of butadiene over TiO_2 supported copper, gold and gold–copper catalysts prepared by deposition–precipitation. *Physical Chemistry Chemical Physics*, 16, 26514-26527. DOI: 10.1039/C4CP02141J.

[8] Suh, Y.-W., Moon, S.-H., Rhee, H.-K. (2000). Active sites in $Cu/ZnO/ZrO_2$ catalysts for methanol synthesis from CO/H_2. *Catalysis Today*, 63, 447-452. DOI: 10.1016/S0920-5861(00)00490-9.

[9] Sun, Y., Sermon, P.A. (1994). Evidence of a metal-support interaction in sol-gel derived $Cu\text{-}ZrO_2$ catalysts for CO hydrogenation. *Catalysis Letters*, 29, 361-369. DOI: 10.1007/BF00807115.

[10] Abaide, E., Anchieta, C., Foletto, V., Reinehr, B., Nunes, L., Kuhn, R., Foletto, E. (2015). Production of copper and cobalt aluminate spinels and their application as supports for inulinase immobilization. *Materials Research*, 18, 1062-1069. DOI: 10.1590/1516-1439.031415.

[11] Kwak, B.K., Park, D.S., Yun, Y.S., Yi, J. (2012). Preparation and characterization of nanocrystalline $CuAl_2O_4$ spinel catalysts by sol–gel method for the hydrogenolysis of glycerol. *Catalysis Communications*, 24, 90-95. DOI: 10.1016/j.catcom.2012.03.029.

[12] Xi, H.J., Li, G.J., Qing, S., Hou, X.N., Zhao, J.Z., Liu, Y.J., Gao, Z. (2013). Cu-Al spinel catalyst prepared by solid phase method for methanol steam reforming. *Ranliao Huaxue Xuebao/Journal of Fuel Chemistry and Technology*, 41, 998-1002.

[13] Chinnadurai, R., Vijaya, J., Kumar R.T., Kennedy, L. (2015). Selective liquid phase oxidation of benzyl alcohol catalyzed by copper aluminate nanostructures. *Journal of Molecular Structure,* 1079, 182. DOI: 10.1016/j.molstruc.2014.09.045.

[14] Tangcharoen, T., T-Thienprasert, J., Kongmark, C. (2018). Optical properties and versatile photocatalytic degradation ability of MAl_2O_4 (M = Ni, Cu, Zn) aluminate spinel nanoparticles. *Journal of Materials Science: Materials in Electronics*, 29, 8995-9006. DOI: 10.1007/s10854-018-8924-4.

[15] Wen, Y., Huang, W., Wang, B. (2012). A novel method for the preparation of Cu/Al_2O_3 nanocomposite. *Applied Surface Science*, 258, 2935-2938. DOI: 10.1016/j.apsusc.2011.11.010.

[16] Shim, J.-O., Na, H.-S., Jha, A., Jang, W.-J., Jeong, D.-W., Nah, I.W., Roh, H.-S. (2016). Effect of preparation method on the oxygen vacancy concentration of CeO_2-promoted $Cu/\gamma\text{-}Al_2O_3$ catalysts for HTS reactions. *Chemical Engineering Journal*, 306, 908-915. DOI: 10.1016/j.cej.2016.08.030.

[17] Morales-Leal, F.J., Rivera De la Rosa, J., Lucio-Ortiz, C.J., Bustos Martínez, D., De Haro Del Rio, D.A., Garza-Navarro, M.A., Garcia, C.D. (2018). Comparison between the catalytic and photocatalytic activities of Cu/Al_2O_3 and TiO_2 in the liquid–phase oxidation of methanol–ethanol mixtures: Development of a kinetic model for the preparation of catalyst. *Applied Catalysis A: General*, 562, 184-197. DOI: 10.1016/j.apcata.2018.05.032.

[18] Wolosiak-Hnat, A., Milchert, E., Grzmil, B. (2013). Influence of parameters on glycerol hydrogenolysis over a Cu/Al_2O_3 catalyst. *Chemical Engineering & Technology*, 36, 411-418. DOI: 10.1002/ceat.201200549.

[19] Azurdia, J.A., Marchal, J., Shea, P., Sun, H., Pan, X.Q., Laine, R.M. (2006). Liquid-feed flame spray pyrolysis as a method of producing mixed-metal oxide nanopowders of potential interest as catalytic materials. Nanopowders along the $NiO–Al_2O_3$ tie line including $(NiO)_{0.22}(Al_2O_3)_{0.78}$, A new inverse spinel composition. *Chemistry of Materials*, 18, 731-739. DOI: 10.1021/cm0503026.

[20] Divband Hafshejani, L., Tangsir, S., Koponen, H., Riikonen, J., Karhunen, T., Tapper, U., Lähde, A. (2016). Synthesis and characterization of Al_2O_3 nanoparticles by flame spray pyrolysis (FSP) - Role of Fe ions in the precursor. *Powder Technology*, 298, 42–49. DOI: 10.1016/j.powtec.2016.05.003.

[21] Betancur Granados, N., Yi, E., Laine, R., Restrepo, O. (2015). $CoAl_2O_4$ Blue nanopigments prepared by liquid-feed flames pyrolysis method. *Matéria (Rio de Janeiro)*, 20, 580-587. DOI: 10.1590/S1517-707620150003.0059.

[22] Kim, M., Hinklin, T.R., Laine, R.M. (2008). Core–shell nanostructured nanopowders along $(CeO_x)_x(Al_2O_3)_{1-x}$ tie-line by liquid-feed flame spray pyrolysis (LF-FSP). *Chemistry of Materials*, 20, 5154-5162. DOI: 10.1021/cm703382x.

[23] Zheng, W., Zou, J. (2015). Synthesis and characterization of blue $TiO_2/CoAl_2O_4$ complex pigments with good colour and enhanced near-infrared reflectance properties. *RSC Advances*, *5*, 87932-87939. DOI: 10.1039/C5RA17418J.

[24] Zarazúa-Villalobos, L., Téllez-Jurado, L., Vargas-Becerril, N., Fantozzi, G., Balmori-Ramírez, H. (2018). Synthesis of magnesium aluminate spinel nanopowder by sol–gel and low-temperature processing. *Journal of Sol-Gel Science and Technology*, 85, 110-120. DOI: 10.1007/s10971-017-4526-5.

[25] Rahmat, N., Yaakob, Z., Pudukudy, M., Rahman, N.A., Jahaya, S.S. (2018). Single step solid-state fusion for $MgAl_2O_4$ spinel synthesis and its influence on the structural and textural properties. *Powder Technology*, 329, 409-419. DOI: 10.1016/j.powtec.2018.02.007.

[26] Chaudhary, R.G., Sonkusare, V.N., Bhusari, G.S., Mondal, A., Shaik, D.P.M.D., Juneja, H.D. (2018). Microwave-mediated synthesis of spinel $CuAl_2O_4$ nanocomposites for enhanced electrochemical and catalytic performance. *Research on Chemical Intermediates,* 44, 2039-2060. DOI: 10.1007/s11164-017-3213-z.

[27] Høj, M., Linde, K., Hansen, T.K., Brorson, M., Jensen, A.D., Grunwaldt, J.-D. (2011). Flame spray synthesis of $CoMo/Al_2O_3$ hydrotreating catalysts. *Applied Catalysis A: General*, 397, 201-208. DOI: 10.1016/j.apcata.2011.02.034.

[28] Meng, L., Zhao, H. (2020). Low-temperature complete removal of toluene over highly active nanoparticles $CuO-TiO_2$ synthesized via flame spray pyrolysis. *Applied Catalysis B: Environmental*, 264, 118427. DOI: 10.1016/j.apcatb.2019.118427.

[29] Strobel, R., Baiker, A., Pratsinis, S.E. (2006). Aerosol flame synthesis of catalysts. *Advanced Powder Technology*, 17, 457-480. DOI: 10.1163/156855206778440525.

[30] Mekasuwandumrong, O., Phothakwanpracha, S., Jongsomjit, B., Shotipruk, A., Panpranot, J. (2011). Influence of flame conditions on the dispersion of Pd on the flame spray-derived Pd/TiO_2 nanoparticles. *Powder Technology*, 210, 328-331. DOI: 10.1016/j.powtec.2011.03.017.

[31] Chaisuk, C., Boonpitak, P., Panpranot, J., Mekasuwandumrong, O. (2011). Effects of Co dopants and flame conditions on the formation of Co/ZrO_2 nanoparticles by flame spray pyrolysis and their catalytic properties in CO hydrogenation. *Catalysis Communications*, 12, 917-922. DOI: 10.1016/j.catcom.2011.01.016.

[32] Klysubun, W., Tarawarakarn, P., Thamsanong, N., Amonpattaratkit, P., Cholsuk, C., Lapboonrueng, S., Wongtepa, W. (2019). Upgrade of SLRI BL8 beamline for XAFS spectroscopy in a photon energy range of 1–13 keV. *Radiation Physics and Chemistry*, 175, 108145. DOI: 10.1016/j.radphyschem.2019.02.004.

[33] Ravel, B., Newville, M. (2005). ATHENA, ARTEMIS, HEPHAESTUS: Data analysis for X-ray absorption spectroscopy using IFEFFIT. *Journal of Synchrotron Radiation*, 12, 537-541. DOI: 10.1107/S0909049505012719.

[34] López-Suárez, F.E., Bueno-López, A., Illán-Gómez, M.J. (2008). Cu/Al_2O_3 catalysts for soot oxidation: Copper loading effect. *Applied Catalysis B: Environmental*, 84, 651-658. DOI: 10.1016/j.apcatb.2008.05.019.

[35] Hannemann, S., Grunwaldt, J.-D., Lienemann, P., Günther, D., Krumeich, F., Pratsinis, S.E., Baiker, A. (2007). Combination of flame synthesis and high-throughput experimentation: The preparation of alumina-supported noble metal particles and their application in the partial oxidation of methane. *Applied Catalysis A: General*, 316, 226-239. DOI: 10.1016/j.apcata.2006.09.034.

[36] Channei, D., Inceesungvorn, B., Wetchakun, N., Phanichphant, S., Nakaruk, A., Koshy, P., Sorrell, C.C. (2013). Photocatalytic activity under visible light of Fe-doped CeO_2 nanoparticles synthesized by flame spray pyrolysis. *Ceramics International*, 39, 3129-3134. DOI: 10.1016/j.ceramint.2012.09.093.

[37] Pisduangdaw, S., Panpranot, J., Chaisuk, C., Faungnawakij, K., Mekasuwandumrong, O. (2011). Flame sprayed tri-etallic Pt–Sn–X/Al_2O_3 catalysts (X = Ce, Zn, and K) for propane dehydration. *Catalysis Communications*, 12, 1161-1165. DOI: 10.1016/j.catcom.2011.04.002.

[38] Kamil, D. (2018). Formation of γ-Al_2O_3 Nanoparticles coating by laser assisted spray pyrolysis and controlled of particle size. *Advances in Environmental Biology*, 9, 132-138.

[39] Tok, A., Boey, F., Zhao, X. (2006). Novel synthesis of Al_2O_3 nano-particles by flame spray pyrolysis. *Journal of Materials Processing Technology*, 178, 270-273. DOI: 10.1016/j.jmatprotec.2006.04.007.

[40] Yu, J., Zhang, Z., Dallmann, F., Zhang, J., Miao, D., Xu, H., Dittmeyer, R. (2016). Facile synthesis of highly active Rh/Al_2O_3 steam reforming catalysts with preformed support by flame spray pyrolysis. *Applied Catalysis B: Environmental*, 198, 171-179. DOI: 10.1016/j.apcatb.2016.05.050.

[41] Volanti, D.P., Keyson, D., Cavalcante, L.S., Simões, A.Z., Joya, M.R., Longo, E., Souza, A.G. (2008). Synthesis and characterization of CuO flower-nanostructure processing by a domestic hydrothermal microwave. *Journal of Alloys and Compounds*, 459, 537-542. DOI: 10.1016/j.jallcom.2007.05.023.

[42] Silva, H., Mateos Pedrero, C., Ribeirinha, P., Boaventura, M., Mendes, A. (2015). Low-temperature methanol steam reforming kinetics over a novel $CuZrD_yAl$ catalyst. *Reaction Kinetics, Mechanisms and Catalysis*, 115, 321-339. DOI: 10.1007/s11144-015-0846-z.

[43] Shishido, T., Yamamoto, Y., Morioka, H., Takaki, K., Takehira, K. (2004). Active Cu/ZnO and Cu/ZnO/Al_2O_3 catalysts prepared by homogeneous precipitation method in steam reforming of methanol. *Applied Catalysis A: General*, 263, 249-253. DOI: 10.1016/j.apcata.2003.12.018.

[44] Ding, J., Chen, J. (2015). Synthesis of Cu-Zn-Zr-Al-O catalyst via a citrate complex route modified by different solvents and their dehydrogenation/hydrogenation performance. *RSC Advances*, 5, 82822-82833. DOI: 10.1039/C5RA13778K.

[45] Chen, L.-F., Guo, P.-J., Zhu, L.-J., Qiao, M.-H., Shen, W., Xu, H.-L., Fan, K.-N. (2009). Preparation of Cu/SBA-15 catalysts by different methods for the hydrogenolysis of dimethyl maleate to 1,4-butanediol. *Applied Catalysis A: General*, 356, 129-136. DOI: 10.1016/j.apcata.2008.12.029.

[46] He, M., Luo, M., Fang, P. (2006). Characterization of CuO species and thermal solid-solid interaction in CuO/CeO_2-Al_2O_3 catalyst by In-situ XRD, Raman spectroscopy and TPR. *Journal of Rare Earths*, 24, 188-192. DOI: 10.1016/S1002-0721(06)60091-4.

[47] Matsuoka, M., Ju, W.-S., Takahashi, K., Yamashita, H., Anpo, M. (2000). Photocatalytic decomposition of N_2O into N_2 and O_2 at 298 K on Cu(I) ion catalysts anchored onto various oxides. The effect of the coordination state of the Cu(I) ions on the photocatalytic reactivity. *The Journal of Physical Chemistry B*, 104, 4911-4915. DOI: 10.1021/jp9940001.

[48] Hahn, J.E., Scott, R.A., Hodgson, K.O., Doniach, S., Desjardins, S.R., Solomon, E.I. (1982). Observation of an electric quadrupole transition in the x-ray absorption spectrum of a Cu(II) complex. *Chemical Physics Letters*, 88, 595-598. DOI: 10.1016/0009-2614(82)85016-1.

[49] Kosugi, N., Kondoh, H., Tajima, H., Kuroda, H. (1989). Cu K-edge XANES of $(La_{1-x}Sr_x)_2CuO_4$, $YBa_2Cu_3O_y$ and related Cu oxides. valence, structure and final-state effects on 1s-4pπ and 1s-4pσ absorption. *Chemical Physics,* 135, 149-160. DOI: 10.1016/0301-0104(89)87014-4.

[50] Basu, S., Sen, A.K. (2020). Dehydration of glycerol with silica–phosphate-supported copper catalyst. *Research on Chemical Intermediates*, 46, 3545-3568. DOI: 10.1007/s11164-020-04161-4.

[51] Sun, D., Yamada, Y., Sato, S. (2015). Efficient production of propylene in the catalytic conversion of glycerol. *Applied Catalysis B: Environmental*, 174-175, 13-20. DOI: 10.1016/j.apcatb.2015.02.022.

[52] Otomo, R., Yamaguchi, C., Iwaisako, D., Oyamada, S., Kamiya, Y. (2019). Selective dehydration of 1,2-propanediol to propanal over boron phosphate catalyst in the presence of steam. *ACS Sustainable Chemistry & Engineering*, 7, 3027-3033. DOI: 10.1021/acssuschemeng.8b04594.